International Journal of Fluid Mechanics & Thermal Sciences
2018; 4(4): 34-44
http://www.sciencepublishinggroup.com/j/ijfmts
doi: 10.11648/j.ijfmts.20180404.11
ISSN: 2469-8105 (Print); ISSN: 2469-8113 (Online)

Enhanced Thermal Energy Transport Through Nanofluid Saturated in Entrapped Porous Triangular Cavities

Muhammad Arshad Siddiqui[1, 2, *], Tariq Javed[2]

[1]Department of Mathematics, Islamabad Model Post Graduate College H-8, Islamabad, Pakistan

[2]Department of Mathematics and Statistics, Faculty of Basic and Applied Sciences, International Islamic University, Islamabad, Pakistan

Email address:
muhammad.phdma20@iiu.edu.pk (M. A. Siddiqui)

To cite this article:
Muhammad Arshad Siddiqui, Tariq Javed. Enhanced Thermal Energy Transport Through Nanofluid Saturated in Entrapped Porous Triangular Cavities. *International Journal of Fluid Mechanics & Thermal Sciences.* Vol. 4, No. 4, 2018, pp. 34-44.
doi: 10.11648/j.ijfmts.20180404.11

Received: January 10, 2019; **Accepted**: February 15, 2019; **Published**: March 7, 2019

Abstract: Numerical simulations are carried out for natural convective flow through nanofluid confined in entrapped triangular porous medium. Inclined walls of cavities are taken as cold while horizontal walls are assumed heated uniformly. Numerical results obtained are shown in terms of flow patterns, isotherms, heat transfer rate and average heat transfer rate against various ranges of physical parameters including solid volume fraction, Porosity parameter, Darcy, Prandtl and Rayleigh numbers. Most of results presented in this article are obtained using nanoparticles of copper because the combination of water-Cu nonofluid returns better heat transfer rate as compared to other combinations (Al_2O_3 and TiO_2). This investigation shows that the Darcy and Rayleigh numbers produce noticeable effects on flow patterns and temperature distribution in both cavities. Increasing Darcy and Rayleigh numbers increase the strength of stream line circulations. Similarly, average Nusselt number along the cold walls of lower triangular enclosure is found increasing function of Darcy and Rayleigh numbers. Further it has been investigated that the local Nusselt number is maximum at edges of horizontal boundaries of the cavities and it decreases while moving toward center from edges.

Keywords: Natural Convection, Nanofluid, Entrapped Cavities, FEM, Porous Media

1. Introduction

The phenomena of natural convection is area of interest for many researchers due its numerous industrial and engineering applications including heating and cooling systems of buildings, food processing, heat exchangers and in many geophysical processes like control of air and water pollution, ground-coupled heat pumps, grain storage and in solar collectors etc.

Study of natural convection through enclosures of various geometrical shapes filled with porous medium is important area of research because it could help the engineers to design highly efficient thermal systems, which is dire need of time. Many investigations in this area have been reported in literature like Varol [1] investigated energy transport through natural convection in hot fluid flow occurring in entrapped porous trapezoidal cavities using Darcy model. He presented numerical solutions for variety of flow parameters and found that local Nusselt numbers are monotonic in upper trapezoidal, and wave shaped in lower trapezoidal for all Rayleigh numbers. Varol et al. [2] has also visualized the free convective heat transfer in non-isothermally heated porous cavity by using the heat lines concept. He applied finite difference method to calculate numerical solutions of governing flow problem using Darcy law for equation of porous media. Results are presented for variety of values of Rayleigh number ($100 \leq Ra \leq 1000$) and aspect ratio ($0.25 \leq AR \leq 1.0$). Yamanaka et al. [3] investigated natural convective heat transfer in liquid gallium for oscillatory widths of Nusselt number. The enclosure was supposed to be heated from bottom side and cooled from top side. The effects of angle of inclination on natural convective heat transfer are presented by Varol et al. [4], when a fluid saturated porous media is placed inside a triangular enclosure. He noticed that the maximum value of average Nusselt number is obtained at an inclination of 330^0 and minimum mean Nusselt number is observed at an inclination of $210^{0,}$ where at inclination of 240^0 lowest flow strength is seen. Magneto convective flow through a square enclosure

saturated with copper-water nanofluid, when left side of the cavity is moving with a constant velocity influenced by circulating cylinder and heat conducting is studied by Bansal and Chatterjee [5]. Sathiyamoorthy and Chamkha [6] examined convective energy transport through a square enclosure when it is filled with electrically conducting liquid gallium influenced by horizontal/vertical magnetic field. In his flow problem, bottom wall is heated uniformly, upper wall is insulated, left wall is linearly while two cases are considered for right vertical wall (i) cold and (ii) linearly heated. Numerical simulations are carried out for modrate Rayleigh number and wide range of Hartman number (Ha=1-100). He found that the Hartman number can control significantly the magnitude of average Nusselt number. Basak et al. [7] considered the natural convective heat transfer contained in a triangular cavity saturated with porous medium, where various thermal conditions are supposed along different boundaries. He applied finite element analysis to compute numerical results against wide range of pertinent parameters including Darcy number ($10^{-5} \leq Da \leq 10^{-3}$), Rayleigh number ($10^3 \leq Ra \leq 10^6$) and Prandtl number ($0.026 \leq Da \leq 10$). Hossain and Alim [8] has worked on non-uniform heating through electrically conducting flow inside a trapezoidal cavity and observed that the average and local Nusselt numbers are strongly dependent on dimensionless parameters and tilt angle of side walls of trapezoidal cavity.

Javed et al. [9] worked on free convection through an electrically conducting flow contained in a triangular enclosure saturated with porous media when it is subject to either uniform or non-uniform heating. They applied finite element method to carry out numerical simulations of governing flow equations and showed effects against wide range of physical flow parameters. Ghaffari et al. [10] investigated the numerical simulations of non-aligned stagnation poin flow. They considered the Brownian and thermophoresis effect of the nanoparticle saturated into non-Newtonian viscoelastic fluid. Irfan et al. [11] examined natural convection influenced by viscous dissipation in stagnation point flow of an electrically conducting nanofluid over a vertical flat plate. Javed et al. [12] presented the influence of magnetic field on free convective heat transfer of nanofluid inside a triangular cavity subjected to either uniform or non-uniform heat. Nithiarasu et al. [13] studied buoyancy driven flow of convective energy transport through fluid saturated porous medium and showed that multicellular flow pattern appears at high Darcy, Raleigh numbers and low Biot number. Convective heat transfer of flow within two entrapped cavities is also visualized by Basak et al. [14]. They examined the flow through hot materials and cavity is assumed as porous triangular in nature. Xu et al. [15] studied a numerical simulations on convection energy transport around horizontal circular cylinder placed in concentric triangular cavity and observed that the energy transport rate changes because of change in inclination angle, constant aspect ratio and cross-section geometry. Sheikhzadeh and Nazari [16] examined convection heat transfer through Al_2O_3–water nanofluid saturated in porous media packed in the square enclosure. The flow problem is modeled using Dacy-Forchheimer model considering insulated top and bottom walls, where one of side walls is taken to be heated and other is taken cold. Numerical simulations are computed using finite volume technique against wide ranges of physical flow parameters including Solid volume fraction, Darcy and Rayleigh numbers. They observed that the Darcy and Rayleigh numbers are helpful to further augment the heat transfer rate in the flow. [17-20] presents significant work of Sheremet et al. in the area of porous medium filled in cavities of various geometrical shapes in the presence of nanofluid.

Flow through nanofluid saturated porous medium is widely used in various applications like waste product cleaning, petroleum and hydrology. Macroscopic characteristics such as relative permeability etc. are often required while modeling flow at continuum level. These characteristics are, generally, hard to achieve. One can possibly work out with some sample based experiments, however such work simply reproduce one group of conditions because the size of the real flow use to be larger that we usually have in experiments. Therefore these experiments generally can not describe variation expected to be present. Therefore, development of physical-based mathematical models are needed which may give fair idea of flow based on experimental data. The literature reviewed reveals that the convective heat transfer through complex geometries in the presence of isotropic porous medium to obtain optimal design of container is an interesting area of research these days and the case of natural convective heat transfer through nanofluid saturated porous media confined in entrapped triangular cavities has not been considered yet according to author's best knowledge. Hence the present investigation contains numerical simulations for natural convective heat transfer through entrapped triangular porous media full of nanofluid, where horizontal sides are subjected to heat uniformly and inclined sides of cavities are taken as cold.

2. Mathematical Model

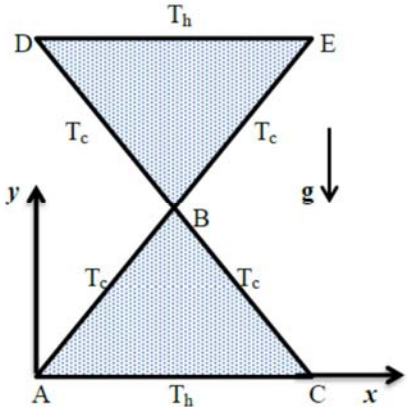

Figure 1. *Graphical representation of the flow problem.*

Configuration considered in this investigation consists of laminar, steady state, two dimensional natural convective

fluid flows within two entrapped triangular porous cavities as represented in Figure 1. The porous media enclosed in entrapped triangular enclosures is full of nanofluid composed of a combination of H_2O and Cu spherical nanoparticles. It is supposed that the horizontal and inclined walls of the enclosures are maintained at uniform temperatures T_h (hot) and T_c (cold) respectively. With the help of Boussinesq approximation [21], variation in the density of fluid with respect to temperature of fluid accounts for a body force term within governing Naver-Stokes equation. Furthermore, local thermal equilibrium (LTE) is valid in this study [22] as temperature of fluid and solid sections in the porous region is equal. The fluid is considered to be incompressible, Newtonian and viscous. The particles of nanofluid are supposed to be in thermal equilibrium within base fluid. In addition to this, there is no slip between particles of nanofluid and base fluid. Thermo-physical properties of water and nanofluid have been represented in Table 1.

Table 1. *Thermo-physical properties of pure water and nanoparticles [23].*

Physical Properties	water	TiO_2	Al_2O_3	Cu
$C_p(J/kgK)$	4179	686.2	765	385
$\rho(kg/m^3)$	997.1	4250	3970	8933
$K(W/mK)$	0.613	8.9538	40	400
$\beta(1/K)$	21×10^{-5}	0.9×10^{-5}	0.85×10^{-5}	1.67×10^{-5}
$\alpha(m^2/s)$	1.47×10^{-7}	30.7×10^{-7}	131.7×10^{-7}	57.45×10^{-7}

Under the above suppositions and by using the laws of conservation of mass, momentum and energy, the governing equation of the current problem might be expressed in dimensional form as

$$u_x + v_y = 0, \tag{1}$$

$$uu_x + vu_y = -\frac{\varepsilon}{\rho_{nf}} p_x + \frac{\mu_{nf}\varepsilon}{\rho_{nf}}\left(u_{xx} + u_{yy}\right) - \varepsilon^2 \frac{\mu_{nf} u}{\rho_{nf} K}, \tag{2}$$

$$uv_x + vv_y = -\frac{\varepsilon}{\rho_{nf}} p_y + \frac{\mu_{nf}\varepsilon}{\rho_{nf}}\left(v_{xx} + v_{yy}\right) + \frac{g(\rho\beta)_{nf}\varepsilon^2}{\rho_{nf}}\left(T - T_c\right) - \varepsilon^2 \frac{\mu_{nf} v}{\rho_{nf} K}, \tag{3}$$

and

$$uT_x + vT_y = \alpha_{nf}\left(T_{xx} + T_{yy}\right). \tag{4}$$

Where *u,* v represents the dimensional velocity components along horizontal and vertical axis respectively, ε is the porosity of the medium and it is supposed to be constant ($\varepsilon = 0.4$), p be the pressure,. The following non-dimensional variables are introduced to non-dimensionalize the governing the boundary value problem

$$\left(X,Y\right) = \left(\frac{x}{L}, \frac{y}{L}\right),\ \left(U,V\right) = \left(\frac{uL}{\alpha_f}, \frac{vL}{\alpha_f}\right),\ P = \frac{pL^2}{\rho_{nf}{\alpha_f}^2},\ \theta = \frac{T - T_c}{T_h - T_c},\ \Pr = \frac{\nu_f}{\alpha_f},\ Ra = \frac{g\beta_f L^3 \Delta T \Pr}{{\nu_f}^2}, Da = \frac{K}{L^2}. \tag{5}$$

We get

$$UU_X + VU_Y = -\varepsilon P_X + \frac{\varepsilon\mu_{nf}}{\rho_{nf}\alpha_f}\left(U_{XX} + U_{YY}\right) - \varepsilon^2 \frac{\mu_{nf} U}{\rho_{nf}\alpha_f Da}, \tag{6}$$

$$UV_X + VV_Y = -\varepsilon P_Y + \frac{\varepsilon\mu_{nf}}{\rho_{nf}\alpha_f}\left(V_{XX} + V_{YY}\right) + \varepsilon^2 \frac{(\rho\beta)_{nf}}{\rho_{nf}\beta_f} RaPr\theta - \varepsilon^2 \frac{\mu_{nf} V}{\rho_{nf}\alpha_f Da}, \tag{7}$$

$$U\theta_X + V\theta_Y = \frac{\alpha_{nf}}{\alpha_f}\left(\theta_{XX} + \theta_{YY}\right). \tag{8}$$

The corresponding boundary conditions in dimensionless form are as follows:

$$\begin{aligned} &U = V = 0, \theta = 0 \text{ at } Y = 0 \text{ and } 0 \le X \le 2, \\ &U = V = 0, \theta = 0 \text{ at } Y = 0 \text{ and } 0 \le X \le 2, \\ &U = 0 = V, \theta = 0 \text{ at } Y - X = 0 \text{ and } 0 \le X, Y \le 2, \\ &U = V = 0, \theta = 0 \text{ at } Y + X = 2 \text{ and } 0 \le X, Y \le 2. \end{aligned} \tag{9}$$

Table 2 represents the properties of nanofluid.

Table 2. *Applied formulation of nanofluid properties [23].*

Nanofluid Properties	Applied Model
Dynamic viscosity	$\mu_{nf} = \frac{\mu_f}{(1-\phi)^{2.5}}$
Heat capacitance	$(\rho c_p)_{nf} = (1-\phi)(\rho c_p)_f + \phi(\rho c_p)_s$
Density	$\rho_{nf} = (1-\phi)\rho_f + \phi\rho_s$
Thermal expansion coefficien	$(\rho\beta)_{nf} = (1-\phi)(\rho\beta)_f + \phi(\rho\beta)_s$
Thermal conductivity	$\frac{k_{nf}}{k_f} = \frac{(k_s+2k_f)-2\phi(k_f-k_s)}{(k_s+2k_f)+\phi(k_f-k_s)}$
Thermal diffusivity	$\alpha_{nf} = \frac{k_{nf}}{(\rho c_p)_{nf}}$

The heat transfer coefficient Nu in non-dimensional form can be obtained for energy transport analysis in natural convective heat transfer in the cavity. The local Nusselt number for entrapped triangular cavities may be defined in terms of temperature field as

(a) For lower triangle

and

$$Nu_h = \frac{k_{nf}}{k_f}\left(\sum_{i=1}^{6}\theta_i\frac{\partial\phi_i}{\partial Y}\right),$$
$$Nu_l = \frac{k_{nf}}{k_f}\left(\sum_{i=1}^{6}\theta_i\left(\frac{1}{\sqrt{2}}\frac{\partial\phi_i}{\partial X}-\frac{1}{\sqrt{2}}\frac{\partial\phi_i}{\partial Y}\right)\right), \qquad (10)$$
$$Nu_r = \frac{k_{nf}}{k_f}\left(\sum_{i=1}^{6}\theta_i\left(\frac{-1}{\sqrt{2}}\frac{\partial\phi_i}{\partial X}-\frac{1}{\sqrt{2}}\frac{\partial\phi_i}{\partial Y}\right)\right).$$

(b) For upper triangle

and

$$Nu_h = \frac{k_{nf}}{k_f}\left(-\sum_{i=1}^{6}\theta_i\frac{\partial\phi_i}{\partial Y}\right),$$
$$Nu_l = \frac{k_{nf}}{k_f}\left(\sum_{i=1}^{6}\theta_i\left(\frac{1}{\sqrt{2}}\frac{\partial\phi_i}{\partial X}+\frac{1}{\sqrt{2}}\frac{\partial\phi_i}{\partial Y}\right)\right), \qquad (11)$$
$$Nu_r = \frac{k_{nf}}{k_f}\left(\sum_{i=1}^{6}\theta_i\left(\frac{-1}{\sqrt{2}}\frac{\partial\phi_i}{\partial X}+\frac{1}{\sqrt{2}}\frac{\partial\phi_i}{\partial Y}\right)\right).$$

The overall heat transfer rate $\overline{Nu}$ was computed by integrating Equations (10) and (11) for the horizontal and inclined walls are as follows

$$\overline{Nu_h} = \frac{\int_0^2 Nu_h dx}{X|_0^2} = \frac{1}{2}\int_0^2 Nu_h dx \text{ and } \overline{Nu_l} = \overline{Nu_r} = \frac{1}{\sqrt{2}}\int_0^{\sqrt{2}} Nu_l dS. \qquad (12)$$

3. Solution Procedure

Galerkin weighted technique is evoked to obtain the solution of momentum and energy equations (6) – (8). Penalty function is used to remove pressure term P from equations (6) and (7) by using penalty parameter γ as

$$P = -\gamma(U_X + V_Y). \qquad (13)$$

For large value of γ, the continuity equation is automatically satisfied. Commonly, the value $\gamma = 10^7$ is taken which yields consistent results. Substituting Equation (12) in Equations (6) and (7), we get

$$UU_X + VU_Y = \gamma\varepsilon\frac{\partial}{\partial X}(U_X + V_Y) + \frac{\mu_{nf}\varepsilon}{\rho_{nf}\alpha_f}(U_{XX} + U_{YY}) - \varepsilon^2\frac{\mu_{nf}U}{\rho_{nf}\alpha_f Da}, \qquad (14)$$

$$UV_X + VV_Y = \gamma\varepsilon\frac{\partial}{\partial Y}(U_X + V_Y) + \frac{\mu_{nf}\varepsilon}{\rho_{nf}\alpha_f}(V_{XX} + V_{YY}) + \varepsilon^2\frac{(\rho\beta)_{nf}}{\rho_{nf}\beta_f}RaPr\theta - \varepsilon^2\frac{\mu_{nf}V}{\rho_{nf}\alpha_f Da}. \qquad (15)$$

By considering 6 nodal triangular elements and bi-quadratic shape functions $\{\phi_k\}_{k=1}^N$, we approximate the non-dimensional velocity components and temperature as follow

$$U \approx \sum_{k=1}^{N} U_k\phi_k(x,y), V \approx \sum_{k=1}^{N} V_k\phi_k(x,y) \text{ and } \theta \approx \sum_{k=1}^{N}\theta_k\phi_k(x,y). \qquad (16)$$

For internal domain Ω, following nonlinear residual equations are obtained after employing Galerkin weighted residual procedure.

$$R_i^1 = \sum_{k=1}^{N} U_k \int_{\Omega} \left[\left(\sum_{k=1}^{N} U_k \phi_k \right) \frac{\partial \phi_k}{\partial X} + \left(\sum_{k=1}^{N} V_k \phi_k \right) \frac{\partial \phi_k}{\partial Y} \right] \phi_i dXdY + \varepsilon\gamma \left[\sum_{k=1}^{N} U_k \int_{\Omega} \frac{\partial \phi_i}{\partial X} \frac{\partial \phi_k}{\partial X} dXdY + \sum_{k=1}^{N} V_k \int_{\Omega} \frac{\partial \phi_i}{\partial X} \frac{\partial \phi_k}{\partial Y} dXdY \right] + \frac{\mu_{nf} \varepsilon}{\rho_{nf} \alpha_f} \sum_{k=1}^{N} U_k \int_{\Omega} \left[\frac{\partial \phi_i}{\partial X} \frac{\partial \phi_k}{\partial X} + \frac{\partial \phi_i}{\partial Y} \frac{\partial \phi_k}{\partial Y} \right] dXdY + \varepsilon^2 \frac{\mu_{nf}}{\rho_{nf} \alpha_f Da} \int_{\Omega} \left[\sum_{k=1}^{N} U_k \phi_k \right] \phi_i dXdY, \tag{17}$$

and

$$R_i^2 = \sum_{k=1}^{N} V_k \int_{\Omega} \left[\left(\sum_{k=1}^{N} U_k \phi_k \right) \frac{\partial \phi_k}{\partial X} + \left(\sum_{k=1}^{N} V_k \phi_k \right) \frac{\partial \phi_k}{\partial Y} \right] \phi_i dXdY + \gamma\varepsilon \left[\sum_{k=1}^{N} U_k \int_{\Omega} \frac{\partial \phi_i}{\partial Y} \frac{\partial \phi_k}{\partial X} dXdY + \sum_{k=1}^{N} V_k \int_{\Omega} \frac{\partial \phi_i}{\partial Y} \frac{\partial \phi_k}{\partial Y} dXdY \right] + \frac{\mu_{nf} \varepsilon}{\rho_{nf} \alpha_f} \sum_{k=1}^{N} V_k \int_{\Omega} \left[\frac{\partial \phi_i}{\partial X} \frac{\partial \phi_k}{\partial X} + \frac{\partial \phi_i}{\partial Y} \frac{\partial \phi_k}{\partial Y} \right] dXdY - \varepsilon^2 \frac{(\rho\beta)_{nf}}{\rho_{nf} \beta_f} Ra \Pr \int_{\Omega} \left[\sum_{k=1}^{N} \theta_k \phi_k \right] \phi_i dXdY + \varepsilon^2 \frac{\mu_{nf}}{\rho_{nf} \alpha_f Da} \int_{\Omega} \left[\sum_{k=1}^{N} V_k \phi_k \right] \phi_i dXdY, \tag{18}$$

$$R_i^3 = \sum_{k=1}^{N} \theta_k \int_{\Omega} \left[\left(\sum_{k=1}^{N} U_k \phi_k \right) \frac{\partial \phi_k}{\partial X} + \left(\sum_{k=1}^{N} V_k \phi_k \right) \frac{\partial \phi_k}{\partial Y} \right] \phi_i dXdY + \frac{\alpha_{nf}}{\alpha_f} \left(\sum_{k=1}^{N} \theta_k \int_{\Omega} \left[\frac{\partial \phi_i}{\partial X} \frac{\partial \phi_k}{\partial X} + \frac{\partial \phi_i}{\partial Y} \frac{\partial \phi_k}{\partial Y} \right] dXdY \right) \phi_i dXdY. \tag{19}$$

Reduced system of nonlinear algebraic equations (17) to (19) is further solved by using Newton Raphson method. After evaluating velocity components, stream function is determined by employing the following relation

$$U = \psi_Y, \text{ and } V = -\psi_X. \tag{20}$$

Equation (20) can be expressed into a single equation as

$$\psi_{XX} + \psi_{YY} = U_Y - V_X. \tag{21}$$

The stream function ψ in terms of velocities can also be approximated by using the following 6-nodal triangular element

$$\psi \approx \sum_{k=1}^{6} \psi_k \phi_k (x, y). \tag{22}$$

The residual form of equation (21) might be expressed as

$$R_i^s = \sum_{k=1}^{N} \psi_k \int_{\Omega} \left[\frac{\partial \phi_i}{\partial X} \frac{\partial \phi_k}{\partial X} + \frac{\partial \phi_i}{\partial Y} \frac{\partial \phi_k}{\partial Y} \right] dXdY + \sum_{k=1}^{N} U_k \int_{\Omega} \phi_i \frac{\partial \phi_k}{\partial Y} dXdY - \sum_{k=1}^{N} V_k \int_{\Omega} \phi_i \frac{\partial \phi_k}{\partial X} dXdY. \tag{23}$$

Since there is no cross flow, therefore no-slip (i.e. $\psi = 0$) condition is valid at the nodes for the boundaries.

Validation

In order to develop the grid independent solution of the discussed problem by using own developed code in MATLAB, the numerical values of the computed overall heat transfer rate $\overline{Nu}$ at the lower horizontal lid is demonstrated in Table 3 against different refinement level of non-uniform initial mesh. It is observed that increase in the number of elements or by increasing the refinement level, the percentage error of the solution with the solution at previous refinement level is decreased. It is as minimum as 1% at the fourth refinement level, therefore throughout the study, third refinement level is used for solution with 2816 number of 6-nodal triangular elements.

Table 3. *Overall heat transfer rate* $\overline{Nu}$ *along bottom wall for various mesh sizes.*

Refinements	Number of Elements	$\overline{Nu_b}$
First	176	6.5082
Second	704	6.6057
Third	2816	6.6879
Fourth	11264	6.7530

Once the grid independence is achieved, the code is further validated against the results of Basak et al. [14] as a limiting case for Ra = $5*10^5$, Pr = 6.2 and Da = 10^{-5}, where heat is provided uniformly from horizontal walls. Comparison revealed that our results are accurate and in good agreement with that of Basak et al. [14] as shown in Figure 2. In Figure 2, left column shows results of Basak et al. [14] and right column contains results obtained by our code.

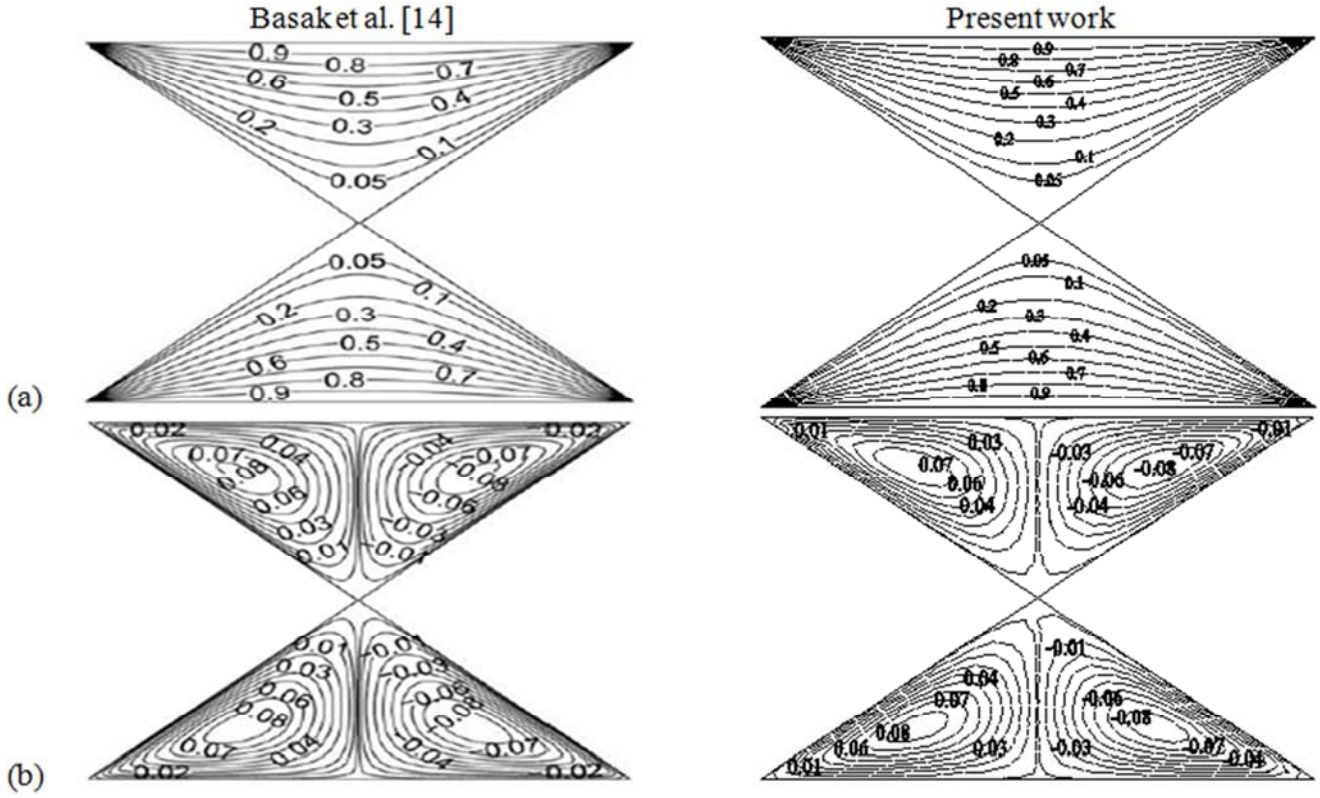

Figure 2. *Streamline and Isotherms contours for Ra=5x10^5, Pr=0.015, Da=10^5 (a) Isotherm lines, (b) Streamlines.*

4. Results and Discussions

This portion of present study contains numerical results and their analysis for free convection through permeable entrapped triangular cavities filled with nanofluid when inclined and horizontal walls are maintained at uniform cold and hot temperatures respectively. The results are obtained and shown in terms of graphs for streamline contours, isotherm contours, heat transfer rate Nu and overall heat transfer rate $\overline{Nu}$ for wide range of involved physical parameters like Da ($10^{-5} \leq Da \leq 10^{-3}$) and Ra ($10^4 \leq Ra \leq 10^7$), while Pr, Porocity ε and Solid volume fraction ϕ are fixed at 6.2, 0.4 and 0.1 respectively.

Figure 3 (a-c) shows graphs for stream line circulations and isotherms contours at Pr=6.2, Da=10^{-4}, ϕ =0.1, ε =0.4 and $10^5 \leq Ra \leq 10^7$. It is evident from this figure that there are significant effects of Raylegh number on flow patterns and heat transfer in the cavity. It is noted that near the center of bottom wall of lower triangle, fluid rises up and after reaching to the top of lower triangle it comes down along inclined walls forming two symmetric rolls of clockwise and counter-clockwise circulations. Similarly two symmetric rolls of concentric circulations are seen in upper triangle also. Here positive values are used to show the heights of counterclockwise circulation contours and negative values are used to show the heights of clockwise circulation contours. Furthermore the increase in Rayleigh number causes increase in the strength of both (clockwise and anticlockwise) circulations where the strength of circulation is increased more significantly in the lower triangle with increase in Rayleigh number as compare to that in upper triangle.

The magnitude of maximum values of stream line contours $|\psi|_{max}$are 0.15, 1 and 4 in upper triangle, 0.15, 3 and 18 in lower triangle for Ra= 10^5, 10^6 and 10^7 respectively as shown in Figure 3 (a-c). On the other hand isotherm contours for small Rayleigh number appears to be smooth and monotonic showing conduction dominant regime as shown in Figure 3 (a). When Rayleigh number is increased to 10^6 isotherms in lower triangle starts stretching upward to top and isotherms in upper triangle gets compressed slightly to top horizontal wall of upper triangle.

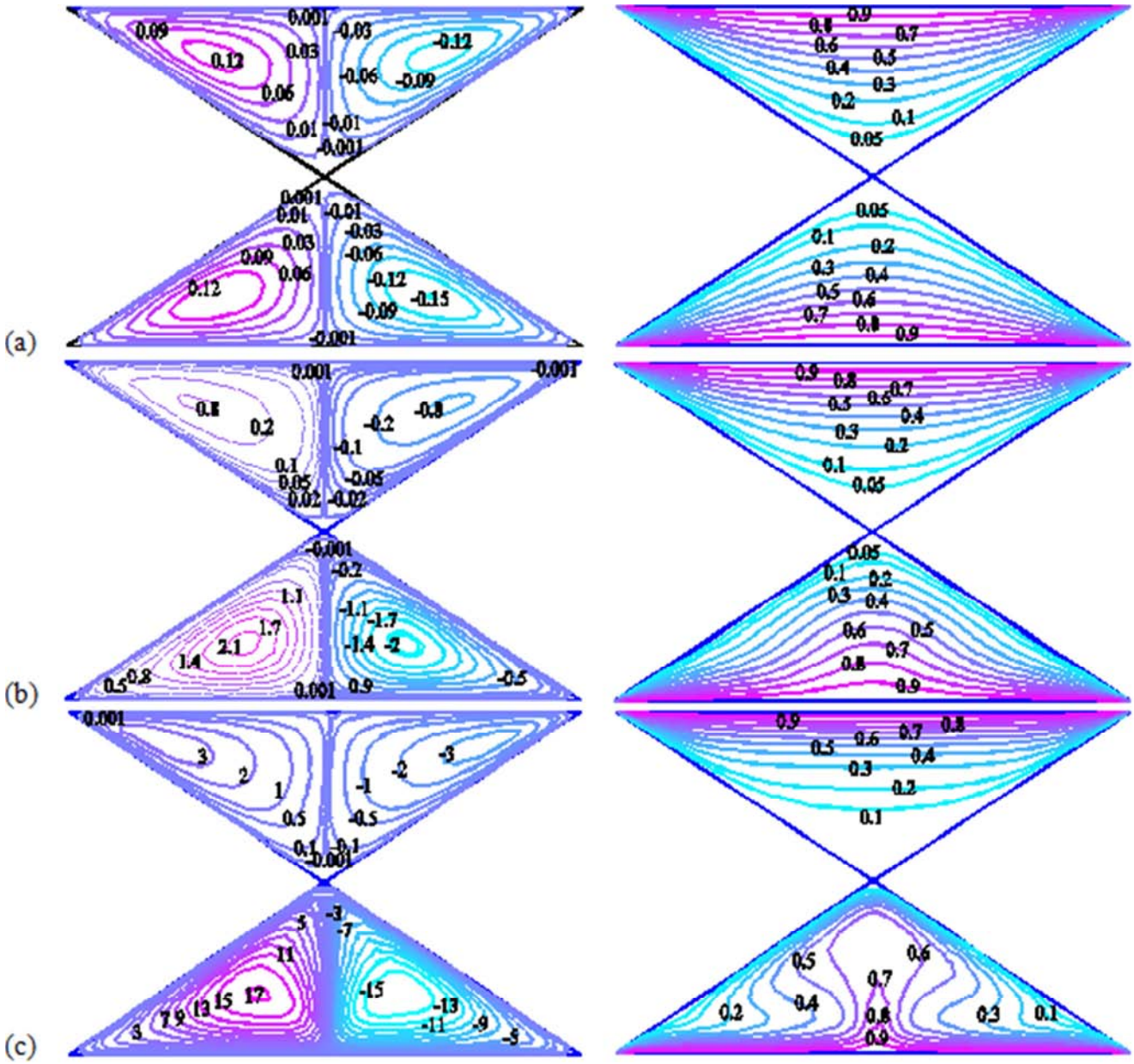

Figure 3. *Streamline and Isotherms contours for Da=10^{-4}, Pr=6.2, $\phi = 0.1, \varepsilon = 0.4$ and (a) Ra=10^5, (b) Ra=10^6, (c) Ra=10^7.*

Increasing Rayleigh number further to 10^7 results into deformed isotherms in lower triangle showing convection dominant effects and a plume like flow pattern is formed in lower triangle where stratification of isotherms is seen near top horizontal wall of upper triangle due to which there were less significant effects on streamline circulation in upper triangle as compared to the effects on streamline circulation in lower triangle. Figure 4 shows graphs for stream line circulation and isotherms contours for two values of Darcy number Da= 10^{-3} and Da=10^{-5} respectively where Ra, Pr, Porosity ε and Solid volume fraction ϕ are fixed at 10^5, 6.2, 0.4 and 0.1 respectively. It is noticed that increase in Darcy number Da results in stronger streamline circulations in both clockwise and anticlockwise directions and change in the values of Darcy number affects circulation contours in lower triangle more prominently. Magnitude of highest value of stream line $|\psi|_{max}$ is noted to be 0.015 and 0.7 in upper triangle and 0.015 & 1.5 in lower triangle for Da= 10^{-3} and 10^{-5} respectively as shown in Figure 4. On the other hand, an isotherm seems to be symmetric about vertical line passing through the center of horizontal walls of upper and lower triangles. It is seen that for small value of Darcy number, isotherms are smooth and monotonically distributed in the enclosure and when Darcy number is increased to 10^{-5} isotherms appears to be slightly pushed upward from near the center of bottom wall in lower triangle while in upper triangle isotherms are compressed a little towards top wall in upper triangle.

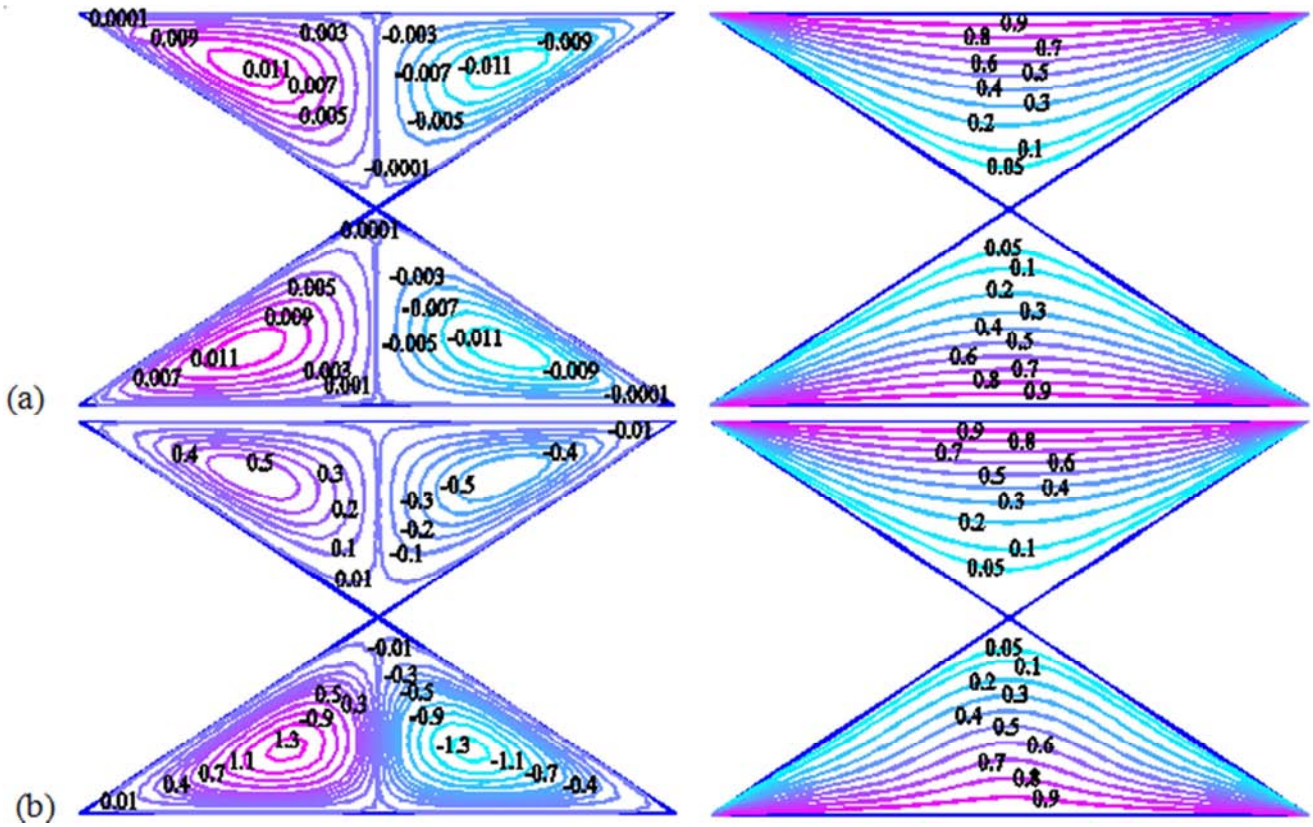

Figure 4. *Isotherms and Streamline contours for Ra=10^5, Pr=6.2, $\phi = 0.1, \varepsilon = 0.4$ and (a) Da=10^{-3}, (b) Da=10^{-5}.*

Figure 5 contains graphs of local Nusselt numbers along horizontal and inclined walls of enclosure against increasing values of distance for three different Rayleigh numbers Ra= 10^5, 10^6 and 10^7 respectively where Prandtl number Pr, Darcy number Da, Porosity ε and solid volume fraction ϕ are fixed at 6.2, 10^{-4}, 0.4 and 0.1. Since horizontal walls of both, upper and lower triangular cavities are considered at a constant temperature (θ =1) while inclined walls are taken cold therefore, there appears a jump type discontinuity at the vertices of horizontal walls of upper and lower triangular cavities. It is due to the fact that the two walls coinciding at these vertices are at different temperature. This discontinuity has been given special attention and is dealt according to Ganzarolli and Milanez [24]. Temperature at these corners nodes is taken to be the average temperature of horizontal and corresponding side walls. However, the adjacent nodes are taken at corresponding boundary wall temperature to avoid singularity. In left column of Figure 5 (a), symmetric distribution of local Nusselt numbers has been observed along the top horizontal wall of upper triangle and value of Nusselt number Nu is noticed to be maximum at both edges of the horizontal wall due to the singularity appearing at these vertices. While moving toward center from this corner, Nusselt number decreases and attains minimum value at the center of horizontal wall. Furthermore increasing Rayleigh number increases local Nusselt numbers monotonically for a fixed value of Distance X near the central area ($0.3 \leq X \leq 1.7$) of horizontal wall and Nu is straight horizontal line in this region for a fixed value of Ra=10^7, where Nusselt numbers for other Rayleigh numbers coincide for $X \leq 0.3$ and $1.7 \leq X$. Similarly for the lower triangle, local Nusselt number is observed maximum at edges of horizontal bottom wall due to the singularity there and it decreases while moving toward center from the corner edges and attains its minimum value at the center of horizontal wall, while for a fixed value of distance X local Nusselt number Nu increases with increasing values of Rayleigh number as shown in right column of Figure 5 (a).

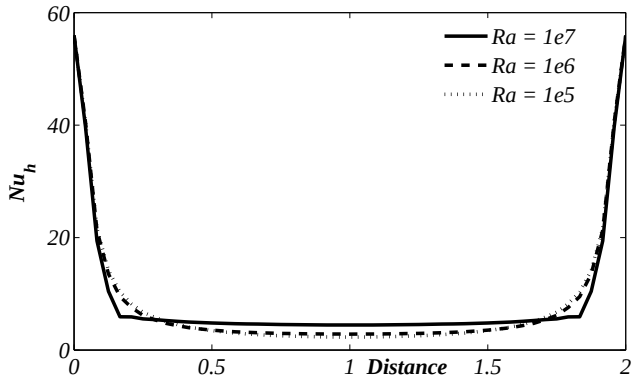

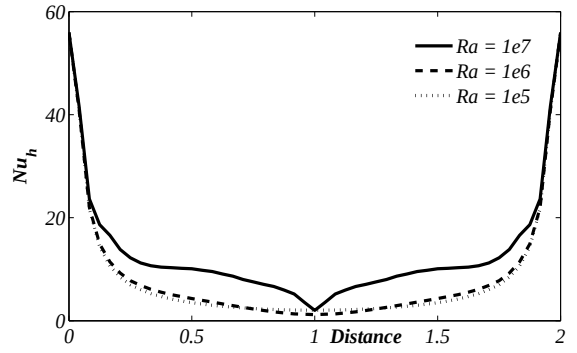

a

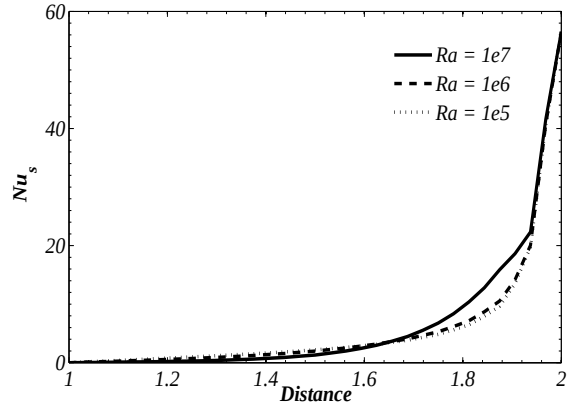

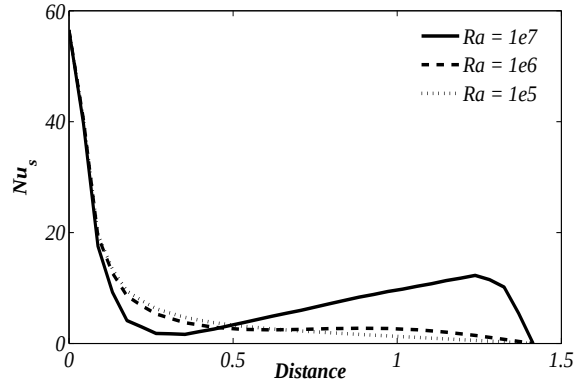

b

Figure 5. *Nusselt number against distance for different values of Ra, where Da=10^{-4}, Pr=6.2, $\phi = 0.1, \varepsilon = 0.4$ and (a) Horizontal wall, (b) Inclined side walls.*

Figure 5 (b) shows local Nusselt numbers along inclined side walls of triangular cavities. Since both inclined walls are taken cold (at the same temperature), therefore curves for both inclined wall are identical and thus we had shown the effects on Nusselt number due to any side walls of each triangular enclosure. It is observed that local Nusselt number Nu_s increases slowly when distance is increased along inclined walls of upper triangular cavity up to 1.8 but Nu_s increases significantly sharp for distance >1.8. However, increasing Rayleigh number increases Nu_s non-significantly up to distance =1.6 and contrarily Nu_s decreases with increase in *Ra* afterwards as shown in left column of Figure 5 (b). While in lower triangular cavity, Nu_s decreases sharply up to distance=0.1 and afterwards it changes slowly with increase in distance for Ra=10^5 and 10^6, but for Ra=10^7 Nu_s increases in the region 0.1<X<1.2 and then it decreases afterwards.

Figure 6 depicts the graphs of average Nusselt numbers for horizontal and inclined walls of upper and lower triangular enclosures against Darcy number Da for various values of porosity ε by keeping other parameters fixed. It is seen from left column of Figure 6 (a) for the upper triangle that the overall heat transfer rate along horizontal wall $\overline{Nu_h}$ first decreases slightly and then increases with increase in Darcy number Da where for a fixed value of Da, overall heat transfer rate $\overline{Nu_h}$ decreases with increase in porosity ε along left half of upper horizontal wall while reverse behavior is seen along right half of this wall. Whereas for lower triangle, overall heat transfer rate $\overline{Nu_h}$ along horizontal wall increases with increase in Darcy number Da and for a fixed value of Da, $\overline{Nu_h}$ increase with increase in porosity parameter ε as shown in righ column of Figure 6 (a). In left column of Figure 6 (b), similar behavior of overall heat transfer rate is seen along inclined side walls of lower triangular enclosure while along the side walls of upper cavity, overall heat transfer rate is observed to increase up to Da=0.2x10^{-3} and then decreases afterwards with increase in Darcy number Da where increasing values of porosity parameter ε increases the overall heat transfer rate $\overline{Nu_s}$ against the entire range of Darcy parameter.

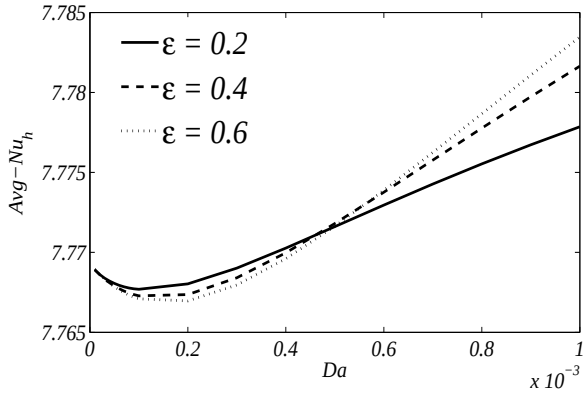

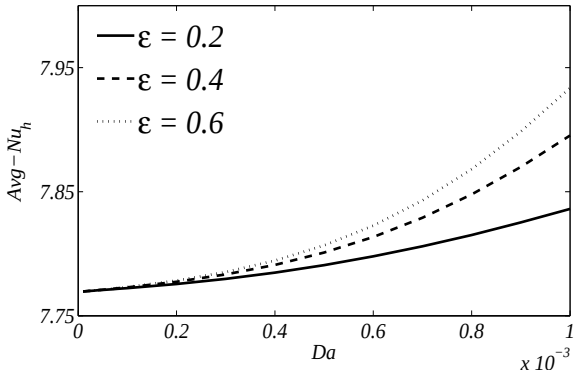

a

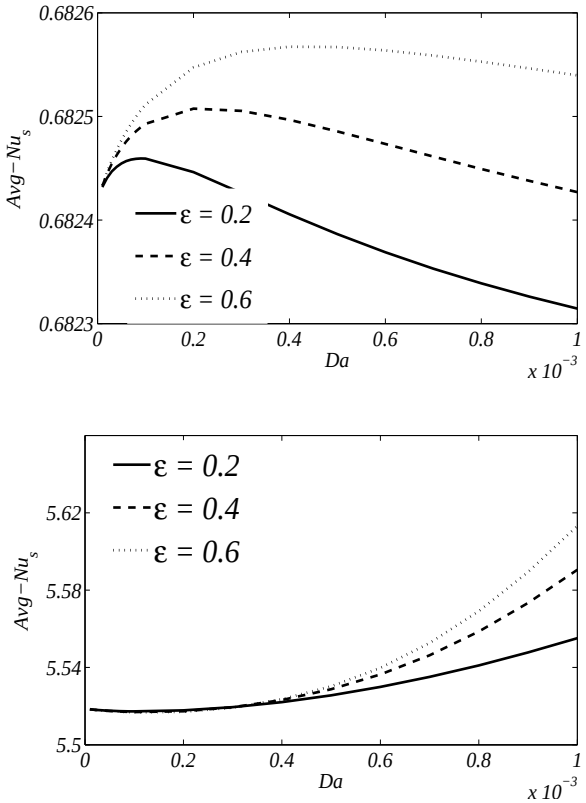

b

Figure 6. *Overall heat transfer rate against Da for various values of porosity (a) Horizontal wall, (b) Inclined side walls where for Ra=10^5, Pr=6.2, ϕ = 0.1.*

Figure 7 (a) shows plots for average Nusselt numbers using combination of water to different nanoparticle including *Cu, TiO_2* and *Al_2O_3* with water as base fluid against increasing values of solid volume fraction ϕ. It has been evidently seen in the figure that increasing solid volume fraction increases the heat transfer rate and comparatively highest heat transfer rate is returned with copper (*Cu)* nano particles. Figure 7 (b) shows the ratio effect of average Nusselt number with different nano particles to the average Nusselt number with *Cu* nano particles $\overline{Nu}/\overline{Nu_C}$ against volume fraction parameter and it is found that the quantitative effects of solid volume fraction ϕ on the ratio $\overline{Nu}/\overline{Nu_C}$ are maximum for the case of *water-Cu* nonofluid.

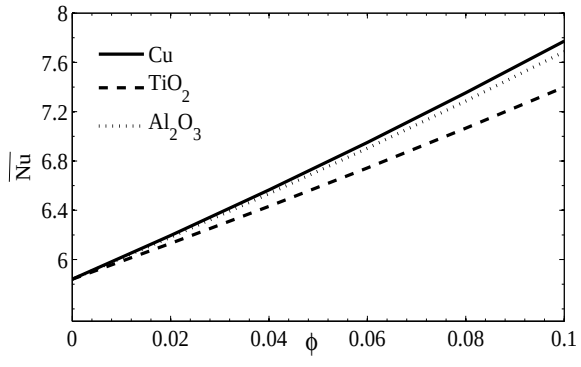

(a)

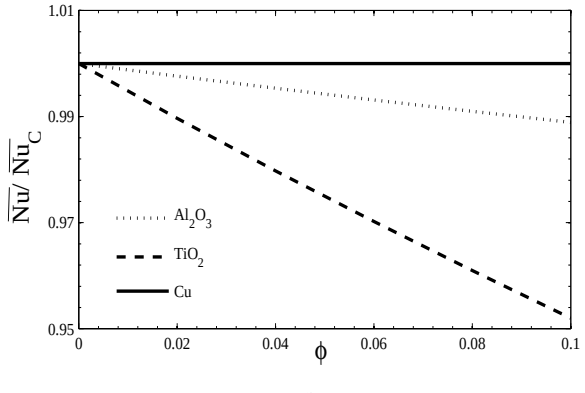

(b)

Figure 7. *(a) Overall heat transfer rate ($\overline{Nu}$) and (b) ratio of overall heat transfer rate to overall heat transfer rate with water-Cu nanoparticles ($\overline{Nu}/\overline{Nu}_c$) against solid volume fraction ϕ for different nanoparticles.*

5. Conclusions

This article deals with natural convection through water-Cu nanofluid saturated in porous medium filled in the enclosure of entrapped triangular cavities, when inclined walls of cavities are considered cold and horizontal walls are taken at constant hot temperature. Obtained results revealed that increase in Rayleigh number increases strength of clockwise and counter clockwise streamline circulation in both the upper and lower triangular cavities. It is noted that more significant effects of Rayleigh number are observed in lower cavity while for small Ra, conduction regime is dominant while for large value of Rayleigh number heat transfers through convection and isotherms are observed to form plume like flow. Similarly increasing Darcy number also increases strength of stream line circulations and comparatively strength of circulation increases more sharply in lower triangular enclosure then that of upper enclosure. Furthermore average Nusselt number is found to be an increasing function of Da along the inclined and horizontal walls of lower cavity. Where along horizontal wall of upper cavity, $\overline{Nu_h}$ increases and along inclined walls $\overline{Nu_s}$ decreases with increase in Da. Local Nusselt number noticed to decreses with increase in distance along inclined wall lower cavity. On the other hand water-Cu nonofluid is observed to returns better heat transfer rate comparing to water-TiO_2 and water-Al_2O_3 nanofluids.

The present investigation has conveyed the useful effects in regard to augmentation in heat transport phenomenon due to presence of copper based nanofluid. The results of the present study are not constrained to the area of energy or heat transport as this type of fluid flow inside a cavity filled with nanofluid can be found in the fields of liquid mixing, food industry and in many others. Furthermore, the present investigation can be extended by considering lid-driven cavity and in the presence of another phenomenon of physics.

References

[1] Y. Varol, Natural convection for hot materials confined within two entrapped porous trapezoidal cavities, International communications in heat and mass transfer 39 (2012) 282-290.

[2] Y. Varol, H. F. Oztop, M. Mobedi, I. Pop, Visualization of natural convection heat transport using heatline method in porous non-isothermally heated triangular cavity, International journal of heat and mass transfer 51 (2008) 5040–5051.

[3] Y. Yamanaka, K. Kakimoto, H. Ozoe, S. W. Churchill, Rayleigh±Benard oscillatory natural convection of liquid gallium heated from below, Chemical engineering journal 71 (1998) 201-205.

[4] Y. Varol, H. F. Oztop, I. Pop, Influence of inclination angle on buoyancy-driven convection in triangular enclosure filled with a fluid-saturated porous medium, Heat mass transfer (2008) 44: 617–624.

[5] S. Bansal, D. Chatterjee, Magneto-convective transport of nanofluid in a vertical lid-driven cavity including a heat-conducting rotating circular cylinder, Numerical heat transfer 68 (2015) 411–431.

[6] M. Sathiyamoorthy, A. Chamkha, Effect of magnetic field on natural convection flow in a liquid gallium filled square cavity for linearly heated side wall(s), International journal of thermal sciences 49 (2010) 1856-1865.

[7] T. Basak, S. Roy, S. K. Babu, I. Pop, Finite element simulations of natural convection flow in an isosceles triangular enclosure filled with a porous medium: Effects of various thermal boundary conditions, International journal of heat and mass transfer 51 (2008) 2733–2741.

[8] M. S. Hossain, M. A. Alim, MHD free convection within trapezoidal cavity with non-uniformly heated bottom wall, International journal of heat and mass transfer 69 (2014) 327–336.

[9] T. Javed, M. A. Siddiqui, Z. Mehmood, I. Pop, MHD natural convective flow in an isosceles triangular cavity filled with porous medium due to uniform/non-uniform heated side walls, Zeitschrift für naturforschung A. 70 (2015) 919–928.

[10] A. Ghaffari, T. Javed, F. Labropulu, Oblique stagnation point flow of a non-Newtonian nanofluid over stretching surface with radiation: a numerical study, Thermal Science (2015), DOI: 10.2298/TSCI150411163G.

[11] I. Mustafa, T. Javed, A. Majeed, Magnetohydrodynamic (MHD) mixed convection stagnation point flow of a nanofluid over a vertical plate with viscous dissipation, Canadian journal of physics 93 (2015) 1365-1374.

[12] T. Javed, M. A. Siddiqui, Z. Mehmood, I. Pop, Effects of uniform magnetic field on the natural convection of water-cu nanofluid in a triangular cavity with uniformly and non-uniformly heated side wall, International Journal of Numerical Methods for Heat and Fluid Flow (2015), DOI: 10.1108/HFF-10-2015-0448.

[13] P. Nithiarasua, K. N. Seetharamub, T. Sundararajanc, Numerical investigation of buoyancy driven flow in a fluid saturated non-Darcian porous medium, International journal of heat and mass transfer 42 (1999) 1205-1215.

[14] T. Basak, S. Roy, D. Ramakrishna, I. Pop, Visualization of heat transport due to natural convection for hot materials confined within two entrapped porous triangular cavities via heatline concept, International journal of heat and mass transfer 53 (2010) 2100–2112.

[15] X. Xu, Z. Yu, Y. Hub, L. Fan, K. Cen, A numerical study of laminar natural convective heat transfer around a horizontal cylinder inside a concentric air-filled triangular enclosure, International journal of heat and mass transfer 53 (2010) 345–355.

[16] G. A. Sheikhzadeh, S. Nazari, Numerical Study of Natural Convection in a Square Cavity Filled with a Porous Medium Saturated with Nanofluid, Transport phenomena in nano and micro scales 1 (2013) 138-146.

[17] Sheremet, M. A. and Trifonova, T. A., "Unsteady conjugate natural convection in a vertical cylinder partially filled with a porous medium", Numerical Heat Transfer, Part A, Vol. 64, (2013), pp. 994–1015.

[18] Sheremet, M. A. and Pop, I., "Natural convection in a wavy porous cavity with sinusoidal temperature distributions on both side walls filled with a nanofluid: Buongiorno's mathematical model", ASME Journal of Heat Transfer, Vol. 137, (2015), pp. 072601.

[19] Sheremet, M. A., Pop, I. and Shenoy, A., "Unsteady free convection in a porous open wavy cavity filled with a nanofluid using Buongiorno's mathematical model", International Communication in Heat and Mass Transfer, Vol. 67, (2015), pp. 66–72.

[20] Sheremet, M. A., Pop, I. and Bachok, N., "Effect of thermal dispersion on transient natural convection in a wavy-walled porous cavity filled with a nanofluid: Tiwari and Das' nanofluid model", International Journal of Heat and Mass Transfer, Vol. 92, (2015), pp. 1053–1060.

[21] P. H. Oosthuizen, and D. Naylor, "An introduction to convective heat transfer analysis", McGraw-Hill, International Edition, (1999).

[22] D. A. Nield, A. Bejan, Convection in Porous Media, third ed., Springer, New York, (2006).

[23] B. Ghasemi, and S. M. Aminossadati. "Periodic natural convection in a nanofluid-filled enclosure with oscillating heat flux", International Journal of Thermal Sciences, Vol. 49(1), (2010): 1-9.

[24] M. M. Ganzarollli, L. F. Milanez, Natural convection in rectangular enclosure heated from below and symmetrically cooled from sides, International journal of heat and mass transfer 38 (1995) 1063-107.